Journal of Sound and Vibration (2001) **242**(2), 197–214
doi:10.1006/jsvi.2000.3036, available online at http://www.idealibrary.com on IDEAL®

IMPLEMENTATION OF NEW TURBULENCE SPECTRA IN THE LIGHTHILL ANALOGY SOURCE TERMS

S. L. Woodruff

Department of Mathematics and School of Computational Science and Information Technology, Florida State University, Tallahassee FL 32306-4120, *U.S.A.*

J. M. Seiner

National Center for Physical Acoustics, University of Mississippi, University, MS 38677, *U.S.A.*

M. Y. Hussaini

School of Computational Science and Information Technology, Florida State University, Tallahassee FL 32306-4120, *U.S.A.*

AND

G. Erlebacher

Department of Mathematics and School of Computational Science and Information Technology, Florida State University, Tallahassee FL 32306-4120, *U.S.A.*

(*Received* 11 *October* 1999, *and in final form* 2 *March* 2000)

The industry-standard MGB approach to predicting the noise generated by a given aerodynamic flow field requires that the turbulence velocity correlation be specified so that the source terms in the Lighthill acoustic analogy may be computed. The velocity correlation traditionally used in MGB computations is inconsistent with a number of basic qualitative properties of turbulent flows. In the present investigation, the effect on noise prediction of using two alternative velocity correlations is examined.

1. INTRODUCTION

The need for reduced noise production by aircraft is understood by all; this need drives an intense research effort into possible means of effecting such reductions (e.g., reference [1]). At the heart of this problem is the need to predict accurately the noise generated by a turbulent flow.

The prediction of the noise generated by a turbulent flow involves three problems: the computation of the underlying turbulent flow field, the prediction of the noise generated by that flow field and the prediction of the propagation of the acoustic waves in the inhomogeneous medium presented by the flow. None of these problems have been satisfactorily resolved. The computation of turbulent flow about realistic geometries at Reynolds numbers of practical interest can only be carried out through the numerical solution of the Reynolds-averaged Navier–Stokes (RANS) equations, coupled with turbulence models that are not always reliable. Direct numerical simulations and large-eddy simulations are important tools for understanding the physics of turbulent flows

0022-460X/01/170197 + 18 $35.00/0

(and the mechanisms by which they generate noise), but they are for the present restricted to relatively simple geometries and, in the case of DNS, low Reynolds numbers, and so are not currently practical for use in the design of, say, jet nozzles. The details of the physical mechanisms by which turbulence generates noise are as yet still unknown, though the Lighthill acoustic analogy [2] permits the expression of the acoustic noise sources in terms of fourth order velocity correlations of the turbulent flow. Computation of the propagation of an acoustic wave in the spatially and temporally inhomogeneous medium that is the turbulent flow field, once the sound has been generated, is also a non-trivial problem, requiring high levels of accuracy to reliably reproduce the phase relationships between waves.

The present work is concerned with the second of these problems. We do not attempt a first-principles analysis of the generation of sound by turbulence, but rather simply to take the present state of the art to the next level by examining the effect of alternative representations for the turbulence spectra in the source terms in the Lighthill analogy. As a representative of the state of the art of practical acoustics computations, we make use of the MGB code developed by Khavaran [3], which employs the Lilley formulation of the acoustic analogy [4] and convective corrections as proposed by Ffowcs-Williams [5].

The changes made in the present investigation are to the representation of the two-point, two-time, velocity correlation, which, in the Khavaran code [3] and traditionally in the MGB formulation [6], is the empirical representation introduced into acoustic work by Ribner [7]. This representation involves the separation of the velocity correlation into a time-dependent factor and a space-dependent factor. Both factors are generally taken as Gaussian functions of their dependent variables. While this representation has been adequate (e.g., reference [3]), there is clearly room for improvement in its agreement with experiment. This representation is also inconsistent with the self-similar nature of the inertial range of turbulence identified by Kolmogorov [8]. It is natural, then, to ask whether alternative representations might be more successful in making accurate acoustic predictions. In the present paper, several alternative representations of the velocity correlation are implemented in the Khavaran code and the effects of these new correlations on acoustic predictions are presented.

The test case for these alternative representations is the Seiner converging–diverging nozzle [9]. This nozzle has an exit diameter of 3·6 in, a design Mach number of 2·0 and a design total temperature of 1680°F. Acoustic and aerodynamic data were reported by Seiner *et al.* [9] for cases with jet total temperatures ranging from 104 to 2200°F. This data provides a means of assessing the accuracy of both the acoustic computation that is the focus of the present work and the aerodynamic computation that provides the input for the acoustic computation. The accuracy of the aerodynamic computation was discussed in detail by Woodruff *et al.* [10] and the results of that paper are employed in the present investigation. Both cold jet (104°F) and hot jet (1550°F) cases are examined in the present work.

The correlation between two velocities at different points and times in a turbulent flow is the essential component of the noise source computation in the MGB formulation. This correlation will be decomposed below in a manner common in turbulence investigations into a spatial spectrum function $Q(k)$ and a wavenumber-dependent time-correlation function $r(k, \tau)$. In the case of the correlation introduced by Ribner [7] used in the MGB formulation, Q is a Gaussian exponential in k and r is a Gaussian exponential independent of k. Two additional functions are introduced in the present work: the Q corresponding to the Kolmogorov spectrum [8] and an r proposed by Kaneda [11] which is consistent with the Kolmogorov inertial-range scalings. Four correlations may be constructed by combining each of the two Q functions with each of the two r functions. One of these four

correlations is the MGB correlation and a second (the Kolmogorov Q combined with the MGB r) is shown below to differ from it only by a multiplicative constant, so we are left with two new correlations to compare against the MGB correlation.

The Q's and r's discussed here are by no means the only possibilities; the purpose of the present work is to make an initial investigation of the effect of different correlations on the predicted noise spectra and so to determine the potential for improvements in noise-prediction capabilities through the use of improved representations of the velocity correlation. It will be seen that the somewhat crude representation of turbulence made by the correlations tried in the present investigation do not, in fact, predict noise particularly well. But they are seen to cause measurable deviations from the MGB results and to improve on the MGB results in some limited respects, at least for the test cases treated here.

Rubinstein and Zhou, in a series of papers [12–14], have also explored the acoustical consequences of realistic inertial range turbulence behavior, addressing such questions as the resulting acoustic scaling laws, the appropriateness of Eulerian and Lagrangian correlations and the development of subgrid noise-generation models for use in conjunction with large-eddy simulations. In work with similar motivations to that reported here, Zhou *et al.* [15] have implemented realistic inertial-range velocity correlations in the MGB formulation and have also seen some improvement in certain aspects of their noise predictions. They work with a physical space, rather than spectral, representation of the velocity correlation and employ different time correlations than those employed here.

Tam and Auriault [16] have recently proposed a different approach to noise prediction which, while also involving an integral representation of the farfield acoustic energy in terms of a nearfield velocity correlation, does not employ the Lighthill acoustic analogy or theoretically motivated velocity correlations. Their method, based on a billiard-ball style kinetic-theory argument, incorporates an experimentally determined anisotropic velocity correlation function and is shown to work well for a number of jet flows. That Tam and Auriault's results are significantly better than those presented here suggests that an anisotropic velocity correlation may be crucial to accurate noise prediction.

2. AERODYNAMIC COMPUTATION

The aerodynamic data required for the acoustic computation is computed using the CFD code ISAAC [17]. ISAAC (Integrated Solution Algorithm for Arbitrary Configurations) is a second-order-accurate finite-volume code for solving the full Navier–Stokes equations. The convective terms are discretized with an upwind scheme based on Roe's flux-splitting algorithm, the diffusion terms are centrally differenced and the system of equations is iterated using an implicit, spatially split, approximate-factorization scheme. The computation is a Reynolds-averaged Navier–Stokes calculation, in which the mean velocity field is found with the aid of two-equation turbulence models. The computations used in this work were performed with a k–ε model [18]. The aerodynamic calculation is described only briefly here. Further details may be found in Woodruff *et al.* [10].

The computational domain is shown in Figure 1 for this axisymmetric aerodynamic computation. The domain is composed of five blocks, with one in the nozzle (61×61 mesh points), one outside the nozzle (61×61 mesh points) and three downstream of the nozzle exit (65×121, 97×121 and 97×121 mesh points). Experimental conditions are used to determine velocity, pressure and temperature boundary conditions for the upstream boundary within the nozzle. An inflow boundary condition with $M = 0{\cdot}05$ is imposed at the upstream boundary outside the nozzle and a subsonic outflow boundary condition is imposed at the downstream boundary. A characteristic boundary condition is imposed at the outside boundaries and the no-slip condition is imposed at all walls.

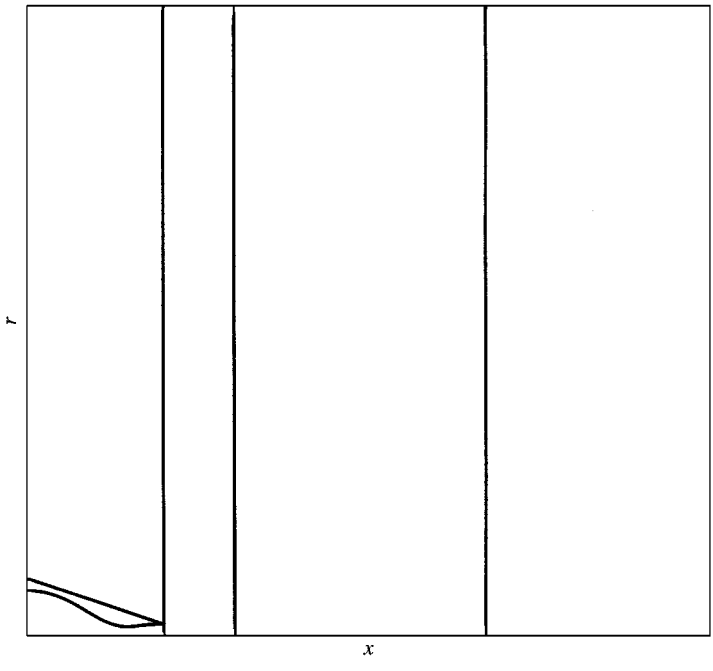

Figure 1. Computational domain.

The first experimental case chosen for the present comparison study is a 104°F case. Results of the aerodynamics computation are shown in Figure 2, taken from Woodruff *et al.* [10], where centerline velocity, Mach number and temperature are compared with the experimental values. The ISAAC results with the k–ε model and using the Sarkar compressibility correction seem to give the best overall agreement with the experimental data; these results will be used as the aerodynamic inputs to the acoustic computations.

The second experimental case chosen for comparison is a 1550°F case. Again, the aerodynamic-computation results are taken from Woodruff *et al.* [10]; they are shown in Figure 3. This time, the ISAAC results with the k–ε model, but without a compressibility correction, give the best overall agreement with experiment and will be used in the acoustic computations.

3. ACOUSTIC COMPUTATION

The acoustic computation is the focus of the present work and is based on the state-of-the-art MGB formulation pioneered by Mani *et al.* [6]. The MGB code upon which the present work is based is that of Khavaran [3]. We give a brief overview of the MGB formulation and the Lighthill acoustic analogy upon which it is based, introduce the new correlations to be examined in this work and compute the noise source spectra that result from these new correlations.

3.1. THE LIGHTHILL ACOUSTIC ANALOGY AND THE MGB FORMULATION

The MGB formulation builds on the Lighthill acoustic analogy as modified by Lilley to produce information about the acoustic field by integrating a Green's-function solution to

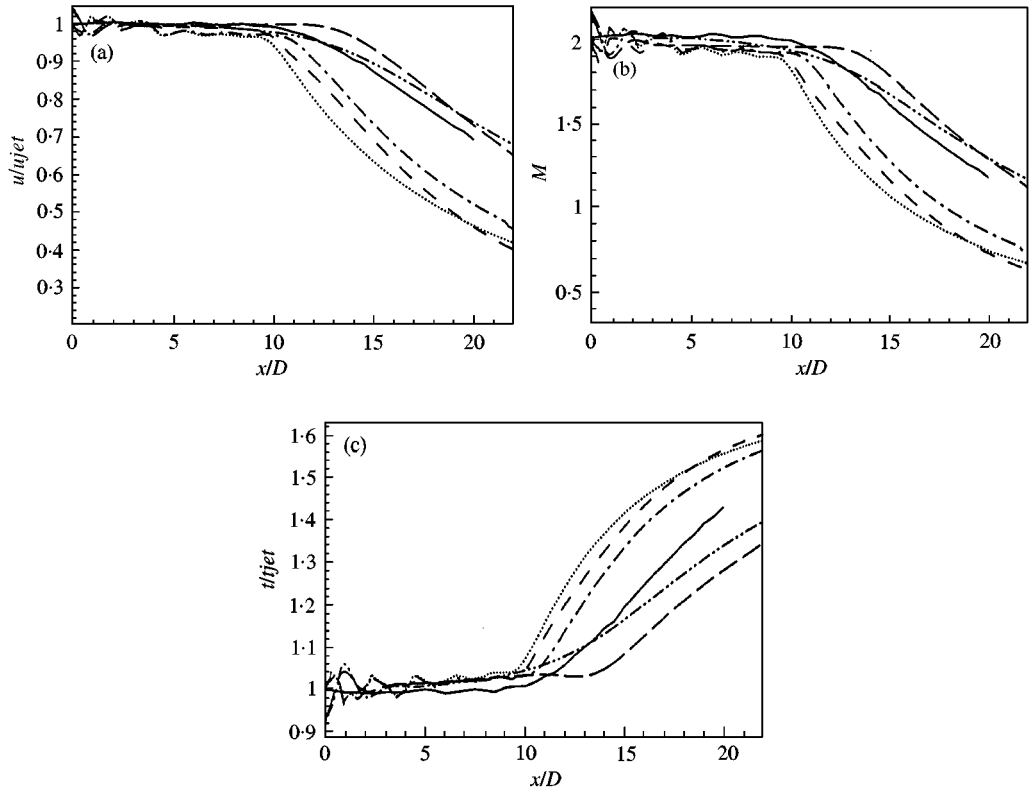

Figure 2. 104°F case, Sarkar compressibility correction: ——, experiment; –·· – ··, ISAAC k–ε model; — —, ISAAC GS ASM; ···, PAB3D k–ε model; –· – ·, PAB3D GS ASM; - - -, PAB3D Girimaji ASM. Centerline (a) velocity, (b) Mach number and (c) temperature.

a wave equation over the turbulent field. Based on what is essentially a ray theory, the code employs high-frequency asymptotic solutions to Lilley's equation coupled with various turbulence approximations and acoustic correction factors to generate solutions for the sound pressure field. The following is concerned with improving the turbulence approximations used in the analysis. By expressing the two-point velocity correlation in a general way, a framework is constructed for experimenting with a variety of velocity correlations more accurate than that used traditionally in MGB formulations. Additionally, the sensitivity of the acoustic results to the accuracy of the turbulence representation may be assessed.

Lighthill [2] expressed the sound pressure level radiated by a turbulent flow in terms of an acoustic source

$$I_{ijkl} = \int \mathrm{d}\xi \frac{\partial^4}{\partial \tau^4} \overline{(\rho v_i v_j)(\rho' v_k' v_l')}, \tag{1}$$

where ξ is the separation vector between the points at which the primed and unprimed quantities are evaluated and τ is the corresponding time difference. The MGB analysis invokes the twin approximations of quasi-incompressibility (the density is assumed constant so that it may be pulled out of the average and out of the integral) and quasi-normality (the resulting average of four velocities is broken up into a sum of products

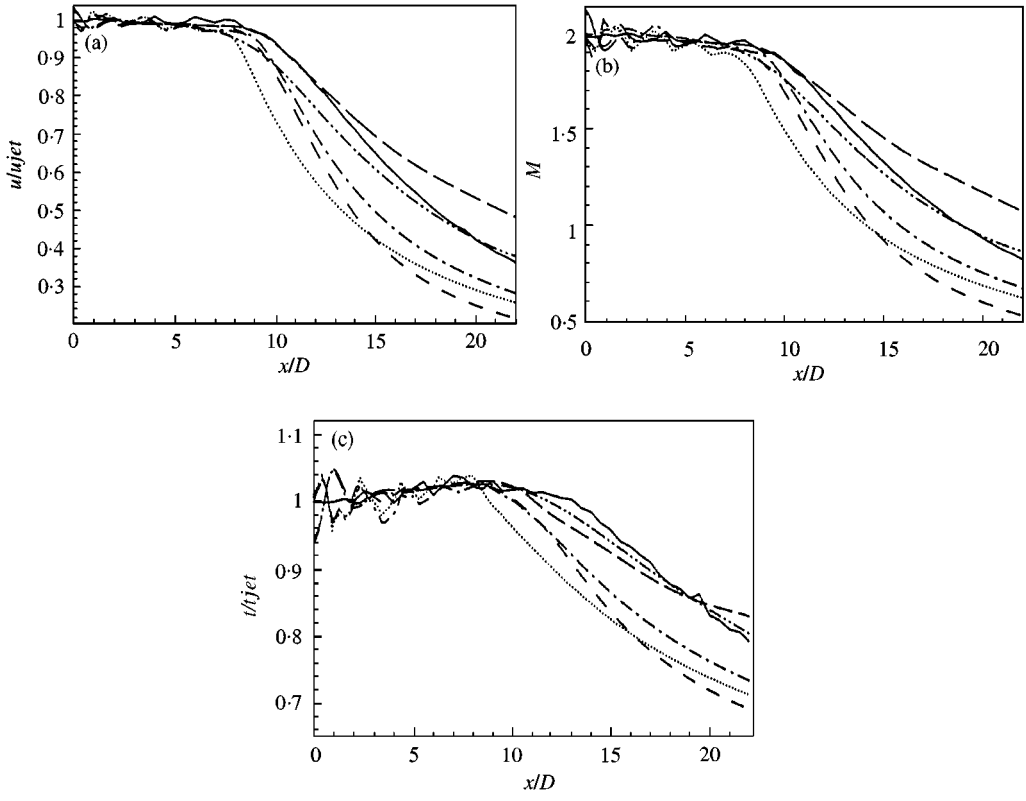

Figure 3. 1550°F case, no compressibility correction: ——, experiment; –·· — ··, ISAAC k–ε model; — —, ISAAC GS ASM; ···, PAB3D k–ε model; –· — · — ·, PAB3D GS ASM; - - -, PAB3D Girimaji ASM. Centerline (a) velocity, (b) Mach number and (c) temperature.

of averages of two velocities). The source then becomes

$$I_{ijkl}(\tau) = \rho^2 \int \mathrm{d}\xi \frac{\partial^4}{\partial \tau^4}(S_{ij}S_{kl} + S_{ik}S_{jl} + S_{il}S_{kj}), \tag{2}$$

with S_{ik}, for example, representing the correlation $\overline{v_i v_k'}$. Assuming, furthermore, that the turbulent flow field is statistically homogeneous, isotropic and stationary at the small scales where the noise is generated, the first term in the integral has no effect since $S_{ij}S_{kl} = \overline{v_i v_j}\,\overline{v_k' v_l'}$ is independent of the time separation τ and its time derivative is zero.

3.2. VELOCITY CORRELATIONS

At this point we depart from the traditional MGB formulation by representing the two-point correlation tensor for a statistically homogeneous, isotropic and stationary turbulent flow in the general form

$$S_{ij}(\boldsymbol{\xi}, \tau) = \int \mathrm{d}\mathbf{k}\, \mathrm{e}^{\mathrm{i}\mathbf{k}\cdot\boldsymbol{\xi}} P_{ij}(\mathbf{k})\, Q(k)\, r(k, \tau). \tag{3}$$

The tensor $P_{ij}(\mathbf{k}) = \delta_{ij} - k_i k_j/k^2$ guarantees that S_{ij} is isotropic and solenoidal, $Q(k)$ is related to the energy spectrum according to

$$Q(k) = \frac{1}{4\pi k^2} E(k) \tag{4}$$

and the function $r(k, \tau)$, describing the temporal correlation at different wavenumbers, is normalized so that $r(k, 0) = 1$. Specific choices of the functions $Q(k)$ and $r(k, \tau)$ will be made below, but the goal here is to construct a framework permitting the acoustic predictions of many choices for these functions to be evaluated. This representation of S_{ij} is common in the theory of turbulence; see, for example, reference [19].

Substitution of the expression for S_{ij} in terms of Q and r in equation (2) yields

$$I_{ijkl}(\tau) = (2\pi)^3 \frac{64\pi}{15} \rho^2 \hat{I}_{ijkl} \int_0^\infty (4\pi k^2 \, \mathrm{d}k) Q^2(k) \frac{\partial^4}{\partial r^4}(r^2(k, \tau)), \tag{5}$$

where

$$\hat{I}_{ijkl} = \frac{15}{64\pi} \int_0^{2\pi} \mathrm{d}\theta \int_0^\pi \mathrm{d}\phi \sin\phi [P_{ik}(\hat{\mathbf{k}}) P_{jl}(\hat{\mathbf{k}}) + P_{il}(\hat{\mathbf{k}}) P_{kj}(\hat{\mathbf{k}})] \tag{6}$$

and

$$\hat{\mathbf{k}} = (\cos\theta \sin\phi, \sin\theta \sin\phi, \cos\phi). \tag{7}$$

It is more convenient to work with the frequency representation for I_{ijkl} (equation (2) Fourier-transformed in time); we then have, since

$$\int_{-\infty}^{+\infty} \mathrm{d}\tau \frac{\partial^4}{\partial \tau^4}(r^2(k, \tau)) \mathrm{e}^{i\Omega\tau} = \Omega^4 \int_{-\infty}^{+\infty} \mathrm{d}\tau (r^2(k, \tau)) \mathrm{e}^{i\Omega\tau}, \tag{8}$$

$$I(\Omega) = \frac{2048\pi^2}{15} \rho^2 \Omega^4 \int_0^\infty \mathrm{d}k [kQ(k)]^2 \int_{-\infty}^{+\infty} [r(k, \tau)]^2 \, \mathrm{e}^{i\Omega\tau} \, \mathrm{d}\tau. \tag{9}$$

In addition, using $\int_0^{2\pi} \mathrm{d}\theta \int_0^\pi \mathrm{d}\phi \sin\phi = 4\pi$, $\int_0^{2\pi} \mathrm{d}\theta \int_0^\pi \mathrm{d}\phi \sin\phi \; \hat{k}_i \hat{k}_j = 4\pi/3 \, \delta_{ij}$ and $\int_0^{2\pi} \mathrm{d}\theta \int_0^\pi \mathrm{d}\phi \sin\phi \; \hat{k}_i \hat{k}_j \hat{k}_l \hat{k}_m = 4\pi/15 (\delta_{ij}\delta_{lm} + \delta_{il}\delta_{jm} + \delta_{im}\delta_{jl})$, we find, after some computation, that

$$\hat{I}_{ijkl} = \frac{1}{16} [7(\delta_{ik}\delta_{jl} + \delta_{il}\delta_{kj}) + 2\delta_{ij}\delta_{kl}]. \tag{10}$$

A variety of choices for $Q(k)$ and $r(k, \tau)$ are available in the turbulence literature and may be conveniently tested with the adapted MGB code. All the choices considered in the present work have a Gaussian form for the temporal correlation, so that the correlation may be written $r(k, \tau) = \exp[-(\tau/\tau_0)^2/\sigma^2(k)]$. In this expression, the function σ is dimensionless and τ_0 is a characteristic time of the turbulence. With u', a characteristic velocity of the large-scale eddies, this characteristic time may be used to non-dimensionalize the source spectrum. The source spectrum for the Gaussian time correlation becomes

$$\frac{I(\Omega)}{\rho^2 u'^7} = \frac{2048\pi^2}{15} \sqrt{\frac{\pi}{2}} (\Omega\tau_o)^4 \int_0^\infty \mathrm{d}p \, p^2 Q^{*2}(p) \sigma(p) \exp[-\sigma^2(p)(\Omega\tau_o)^2/8], \tag{11}$$

where we define $p = u'\tau_o k$ and

$$Q^*(p) = \frac{Q(k)}{u'^5 \tau_o^3}. \tag{12}$$

Equation (11) provides us with a convenient expression for evaluating the source spectra corresponding to specific velocity correlations.

In the present investigation, two different choices for Q and for r are examined. The first of these are those corresponding to the MGB correlation. The MGB time-correlation function [3] is

$$r_{MGB}(k, \tau) = \mathrm{e}^{-(\tau/\tau_0)^2}, \tag{13}$$

and so the corresponding σ is $\sigma_{MGB}(p) = 1$. The spatial correlation function employed in the MGB formulation, a Gaussian exponential in the separation distance, Fourier transforms to a Gaussian exponential in the wavenumber k and we have

$$Q_{MGB}(k) = \frac{1}{2}(2\pi)^{-4} u'^2 L_x^5 k^2 \mathrm{e}^{-L_x^2 k^2/4\pi} \tag{14}$$

or

$$Q^*_{MGB}(p) = \frac{1}{2}(2\pi)^{-4} a_L^5 p^2 \mathrm{e}^{-a_L^2 p^2/4\pi}. \tag{15}$$

Here L_x is the integral length scale of the turbulence, characterizing the size of the large-scale turbulent motion. As such, it is related to the velocity and time scales u' and τ_o by the relation $L_x = a_L u' \tau_o$, where a_L is a constant.

The second pair of functions Q and r to be examined here are chosen specifically to reproduce the self-similar structure of the Kolmogorov inertial range. Thus, Q and the corresponding Q^* are power laws consistent with the $-5/3$ Kolmogorov inertial-range energy spectrum:

$$Q_K(k) = \frac{1}{4\pi k^2} C_K \varepsilon^{2/3} k^{-5/3}, \quad Q^*_K(p) = \frac{1}{4\pi p^2}\left(\frac{3}{2}\right)^{2/3} \alpha_f^{-2/3} C_K p^{-5/3}. \tag{16}$$

The constant C_K is the Kolmogorov constant, to which we will give the value 1·6, consistent with experimental observations [20]. The turbulent dissipation, ε, may be related to the kinetic energy K $(= 3/2\, u'^2)$ and to the time scale of the large-scale turbulence by dimensional analysis to give $\varepsilon = \tau_o/\alpha_f K$. This relation has been employed by Khavaran [3] to fix the time scale in his MGB code and will be used throughout the present paper. We follow Khavaran in adopting the value $\alpha_f = 2$.

The singular nature of equation (16) as k tends to zero necessitates that the large-scale behavior of Q be adjusted in order to get a usable noise source spectrum. We adopt here a simple and very crude cut-off of the energy spectrum at a wavenumber $k = k_o$, so that the value of $Q(k)$ is taken to be zero if $k < k_o$. It is reasonable to take the previously defined length L_x as the cut off, so $k_o = 2\pi/L_x$. The corresponding cut-off value for the function $Q^*(p)$ is $p_o = 2\pi/a_L$.

We now describe a time-correlation function $r(k, \tau)$ that is more faithful to true turbulence dynamics than the function given in equation (13). Such a time-correlation function must reflect the fact that the characteristic correlation times of different-sized motions are different; thus the dependence of $r(k, \tau)$ on the wavenumber k, which the MGB

correlation r_{MGB} lacks, is crucial. Broadly speaking, $r(k, \tau)$ should reflect the fact that small-scale motion decorrelates faster than large-scale motion. Dimensional analysis in the inertial range [8] leads more specifically to the scaling relationship $\tau \sim k^{-2/3}$. Kaneda [11] has presented an inertial-range time-correlation function consistent with this scaling and with experimental data:

$$r_K(k, \tau) = \mathrm{e}^{-\pi\sigma_o^2(\varepsilon^{1/3}k^{2/3}\tau)^2/4}. \tag{17}$$

The constant σ_o takes the value 0·9. As this function is again a Gaussian exponential, it may be expressed in the form presented in the previous subsection, with

$$\sigma_K(p) = \frac{2\alpha_f^{1/3}}{(3/2)^{1/3}(\sqrt{\pi})\sigma_o} p^{-2/3}. \tag{18}$$

The above expressions have all been manipulated so that the only free parameters in the velocity correlations are the characteristic velocity and time, u' and τ_o. The only constant left undetermined in the course of these manipulations was a_L, in the relation between the length L_x and u' and τ_o. We are not necessarily free to choose a_L as we please, such as by appealing to experimental results, because it is necessary by definition that the energy spectrum $E(k) = 4\pi k^2\, Q(k)$ satisfy the relation $\int_0^\infty \mathrm{d}k\, E(k) = K$. Since $K = \frac{3}{2}u'^2$, this relation should work out to be a simple identity, with all parameters cancelling out. This is the case for the MGB energy spectrum, but is only true for the Kolmogorov energy spectrum if a_L is given by

$$a_L = \frac{4\pi}{3}\alpha_f C_K^{-3/2}. \tag{19}$$

Since α_f and C_K have already been specified above, this relation fixes a_L to a value which we will use throughout this paper.

It remains only to fix precisely τ_o and u' to complete the specification of the velocity correlations to be examined in this paper. The relation following equation (16) is used not only to eliminate ε from Q_K and r_K so that all expressions are written solely in terms of the two parameters τ_o and u', but also as the definition of τ_o in terms of K and ε [3], which are available to the MGB code from the aerodynamic input data. Similarly, given $K = \frac{3}{2}u'^2$, u' may also be determined from the input data.

Before proceeding, it is useful to compare the two energy spectra and the two time-correlation functions in order to better understand the noise spectra that will result. In Figure 4, the two energy spectra are shown normalized by the total kinetic energy so that the area under each of the curves is unity. The non-dimensional wavenumber $p = u'\tau_o k$ was defined above. The MGB spectrum is seen to be composed of wavenumber components in a fairly narrow band centered approximately about the non-dimensional wavenumber corresponding to the length scale L_x, $p_o = 2\pi/a_L \approx 1{\cdot}5$. In contrast, the Kolmogorov energy spectrum is much broader and involves significant contributions from higher wavenumbers.

Both time-correlation functions examined in this paper are Gaussian functions of time; they differ in that the width of the bell curve varies with wavenumber in the case of the Kaneda time correlation. For the parameter values chosen above, $r_K(k, \tau)$ is virtually identical to $r_{MGB}(k, \tau)$ when k is at the cutoff value k_o. As the wavenumber increases, $r_K(k, \tau)$ drops off faster in time so that the correlation time becomes smaller according to $\tau \sim k^{-2/3}$.

There is no reason why Kaneda's r function should not be used with the MGB energy spectrum; this $k^2\mathrm{e}^{-\mathrm{const.}k^2}$ energy spectrum is a common choice for fitting low-Reynolds-number experimental data and initializing low-Reynolds-number DNS runs. It will thus

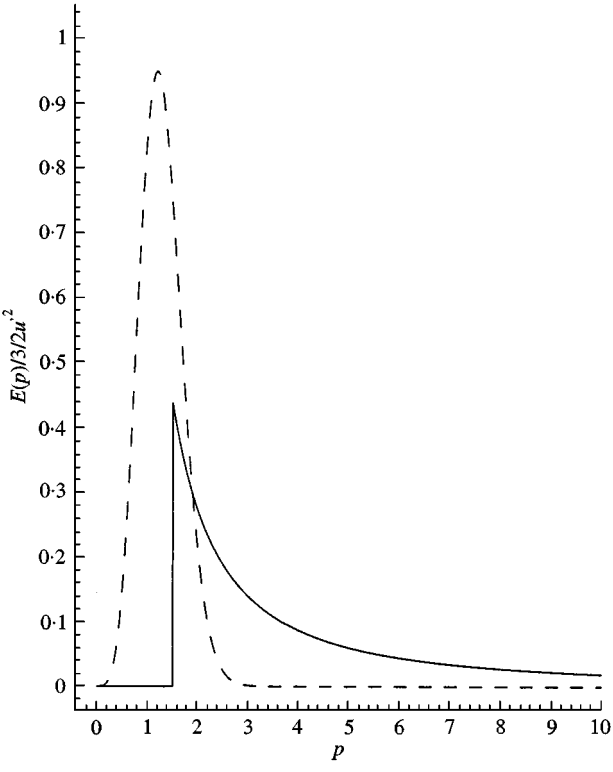

Figure 4. Energy spectra normalized by total kinetic energy: - - -, MGB energy spectrum, $(E(p)/(3/2u'^2) = (12\pi^3)^{-1} a_L^5 p^4 \exp(-a_L^2 p^4/4\pi))$; ——, Kolmogorov energy spectrum, $(E(p)/(3/2u'^2) = (2/3)^{1/3}\alpha_f^{-2/3} C_K p^{-5/3} H(p - p_0))$.

provide an opportunity to compare an essentially low-Reynolds-number correlation with our other, high-Reynolds-number, inertial-range-dominated, Kolmogorov-spectrum-based correlation. So, in addition to the new velocity correlation constructed with the Q_K and r_K (which shall be referred to as the K + K correlation), we have a second new velocity correlation constructed with Q_{MGB} and r_K (to be referred to as the M + K correlation). Noise predictions using these two new correlations will be compared with predictions using the traditional MGB correlation (Q_{MGB} combined with r_{MGB}, or M + M). A fourth correlation results from using Q_K with the MGB time correlation r_{MGB}, but, as mentioned above, this correlation leads to a source spectrum identical to that associated with the M + M correlation, except for a multiplicative constant.

3.3. COMPUTATION OF THE SOURCE SPECTRA

We begin our computation of source spectra corresponding to specific turbulence correlations by recovering the MGB noise spectrum by using Q_{MGB} and r_{MGB} in the determination of $I(\Omega)$. If σ in equation (11) is replaced by σ_{MGB}, but Q is left unspecified, the source spectrum becomes

$$\frac{I(\Omega)}{\rho^2 u'^7} = \frac{2048\pi^2}{15}\sqrt{\frac{\pi}{2}}\left[\int_0^\infty \mathrm{d}p\, p^2 Q^{*2}(p)\right](\Omega\tau_o)^4 \exp[-(\Omega\tau_o)^2/8], \tag{20}$$

and we see that the source spectrum for this choice of time correlation always has a frequency dependence const. $\Omega^4 e^{-\text{const.}\Omega^2}$. The spatial correlation, determined by $Q(k)$, serves only to fix the overall multiplicative constant. Consequently, not only is the MGB expression for the turbulence spectrum unable to represent the inertial range properly, but it always gives a Gaussian frequency dependence multiplied by an algebraic factor and is essentially unaffected by the nature of the spatial correlation. Use of the Kolmogorov Q or any other Q in place of Q_{MGB} does not lead to a significantly different noise spectrum as long as the MGB time correlation is used.

Since we do want to fix the constant in the MGB case, we substitute Q_{MGB} for Q in the above to get the MGB result

$$\frac{I(\Omega)}{\rho^2 u'^7} = \pi^{-3/2} a_L^3 (\Omega \tau_o)^4 e^{-(\Omega\tau_o)^2/8}. \tag{21}$$

The first alternative to the MGB velocity correlation is the K + K correlation, where $Q = Q_K$ and $\sigma = \sigma_K$ are used in equation (11). If the integration is performed without using the cutoff at $k = k_0$ discussed in the previous subsection, one finds

$$\frac{I(\Omega)}{\rho^2 u'^7} \sim (\Omega \tau_0)^{-7/2}. \tag{22}$$

This is a reasonable result for the inertial range and has the self-similar power-law behavior one expects. However, its failure to drop off to zero at low frequencies makes it an inadequate representation of the source spectrum as a whole and makes it unusable in the MGB code.

When the cut off (which has the effect of changing the lower limit of integration in equation (11) to $p_0 = u'\tau_0 k_0 = 2\pi/a_L$) is introduced, the source spectrum becomes, instead of equation (22),

$$\frac{I(\Omega)}{\rho^2 u'^7} = \frac{18}{5} 2^{5/6} 3^{1/3} \pi^{5/3} \left(\frac{a_L}{\alpha_f}\right)^{7/3} \sigma_0^3 C_K^2 f_K \left[\frac{(a_L^2 \alpha_f)^{1/3} \tau_0 \Omega}{2^{5/6} 3^{1/3} \pi^{7/6} \sigma_0}\right]. \tag{23}$$

The function $f_K(z)$ is defined by

$$f_K(z) = z^{-7/2} \left[\Gamma\left(\frac{15}{4}\right) - \Gamma\left(\frac{15}{4}, z^2\right)\right], \tag{24}$$

where $\Gamma(a)$ and $\Gamma(a, x)$ are the Euler gamma function and the incomplete Euler gamma function, respectively.

The second source-spectrum alternative arises from using the M + K velocity correlation. When Q_{MGB} and σ_K are used in equation (11), the source spectrum becomes

$$\frac{I(\Omega)}{\rho^2 u'^7} = \frac{64 a_L}{5\alpha_f} \pi^{5/2} \sigma_0^3 f_e \left[\frac{(a_L^2 \alpha_f)^{1/3} \tau_0 \Omega}{2^{1/2} 3^{1/3} \pi^{5/6} \sigma_0}\right]. \tag{25}$$

The function $f_e(z)$ is defined by

$$f_e(z) = z^4 \int_0^\infty dp'\, p'^{16/3} \exp(-z^2/p'^{4/3} - p'^2). \tag{26}$$

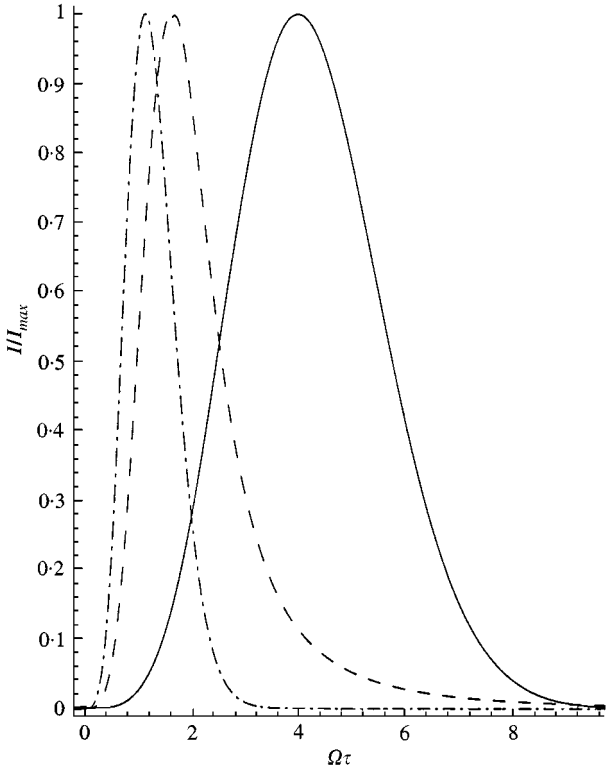

Figure 5. $I(\Omega)/I_{max}$ for the three noise spectra: ——, MGB; - - -, Kolmogorov energy spectrum with Kaneda time correlation (K + K); –· – ·, MGB energy spectrum with Kaneda time correlation (M + K).

We now have three source spectra to consider: the original MGB spectrum of equation (21), the K + K spectrum of equation (23) and the M + K spectrum of equation (25). When these three expressions for $I(\Omega)$ are evaluated numerically, the most dramatic difference between them is in their magnitudes. With the parameter values given in the previous subsection, the MGB spectrum has a peak value 441·31 $\rho^2 u'^7$, the K + K spectrum has a peak value of 2·6 $\rho^2 u'^7$ and the M + K spectrum has a peak value of 15·07 $\rho^2 u'^7$. The three spectra, normalized by their peak values, are shown in Figure 5. The two new spectra are seen to be significantly more narrow-banded than the MGB spectrum and to peak at lower frequencies: at $\Omega\tau_0 = 1{\cdot}65$ for the K + K spectrum and $\Omega\tau_0 = 1{\cdot}15$ for the M + K spectrum, in contrast to the $\Omega\tau_0 = 4$ peak of the MGB spectrum.

4. RESULTS

The effects on actual noise predictions of using the new source spectra instead of the standard MGB form are now examined. Results are compared with experiment for the two experimental cases described previously. As discussed in the aerodynamics-computation section, the aerodynamic data used for the 104°F jet case is computed using ISAAC with the k–ε model with the Sarkar compressibility correction, and the aerodynamics data used for the 1550°F jet case is computed using ISAAC with the k–ε model without the Sarkar compressibility correction.

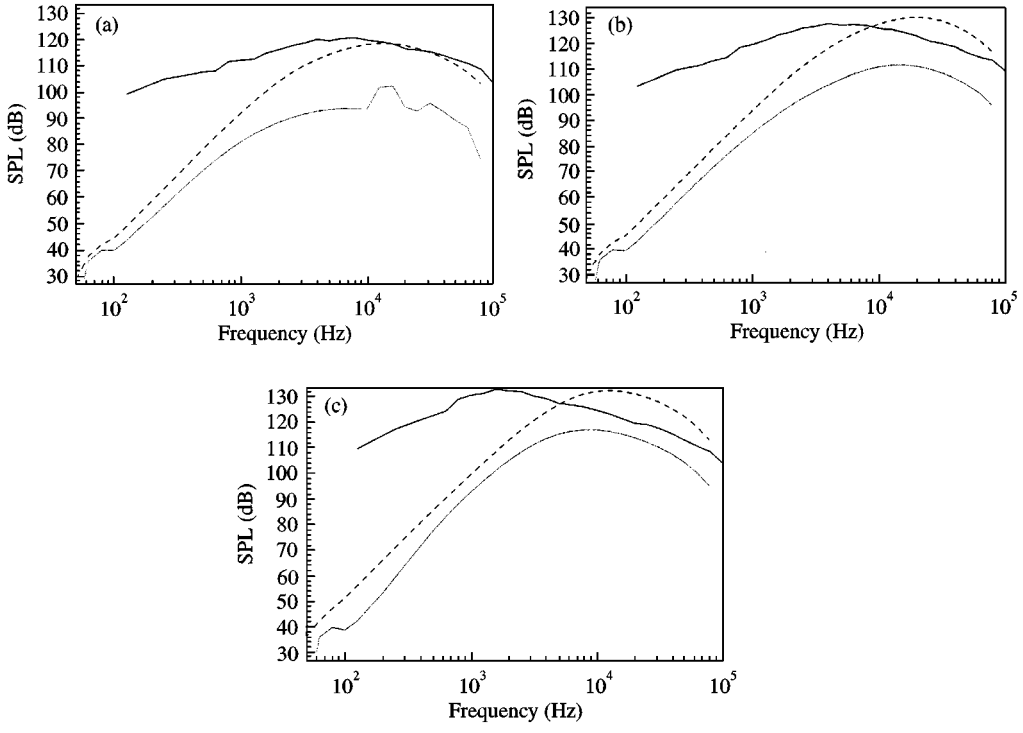

Figure 6. SPL at three microphone angles for 104°F case: ——, experiment; - - -, Khavaran MGB code; ⋯, present computation, using Kolmogorov spectrum and Kaneda time correlation (K + K). (a) $\theta = 93{\cdot}3^\circ$, (b) $\theta = 122{\cdot}7^\circ$ and (c) $\theta = 138{\cdot}8^\circ$.

The experimental acoustic data was taken with a series of microphones located on a line parallel to the jet axis and 12 ft from that axis. For the present comparison, sound pressure levels (SPLs) in one-third-octave bands are given at each of three microphone positions. For each microphone position, the experimental SPL, the SPL given by the traditional MGB formulation and the SPL given by the new source spectrum is displayed. The angle θ is the angle between a line from the jet nozzle to the microphone and the jet axis, measured so the 180° is directly downstream of the nozzle and 90° is abeam of it.

Figure 6 shows results for the 104°F case, using the source spectrum of equation (23) from the K + K velocity correlation. The predictions of the new source spectrum are significantly lower than those of the MGB source spectrum, as might be expected given the much smaller amplitude of this source spectrum. The sharp peaks that appear in the $\theta = 93{\cdot}3^\circ$ SPL at high frequency are the result of contributions from other noise mechanisms (such as shock noise); the MGB source spectrum contribution is large enough that these other contributions play no significant role for this test case. (Note that one would not expect shock noise to make a significant contribution to noise generation for this test case.) It is encouraging that the SPL as a whole is broader than the MGB SPL, particularly for the $\theta = 93{\cdot}3^\circ$ case, and in this respect agrees better with experiment. It is also of interest that the experimental results are marked by a reduction in the frequency of the SPL peak as θ increases. While neither prediction reflects this property well, the peaks in the SPLs associated with the K + K correlation move more than those of the MGB SPLs. (The altered source frequency spectrum is able to affect the angular dependence of the noise predictions because it emphasizes different frequency bands. The amplitude of the different

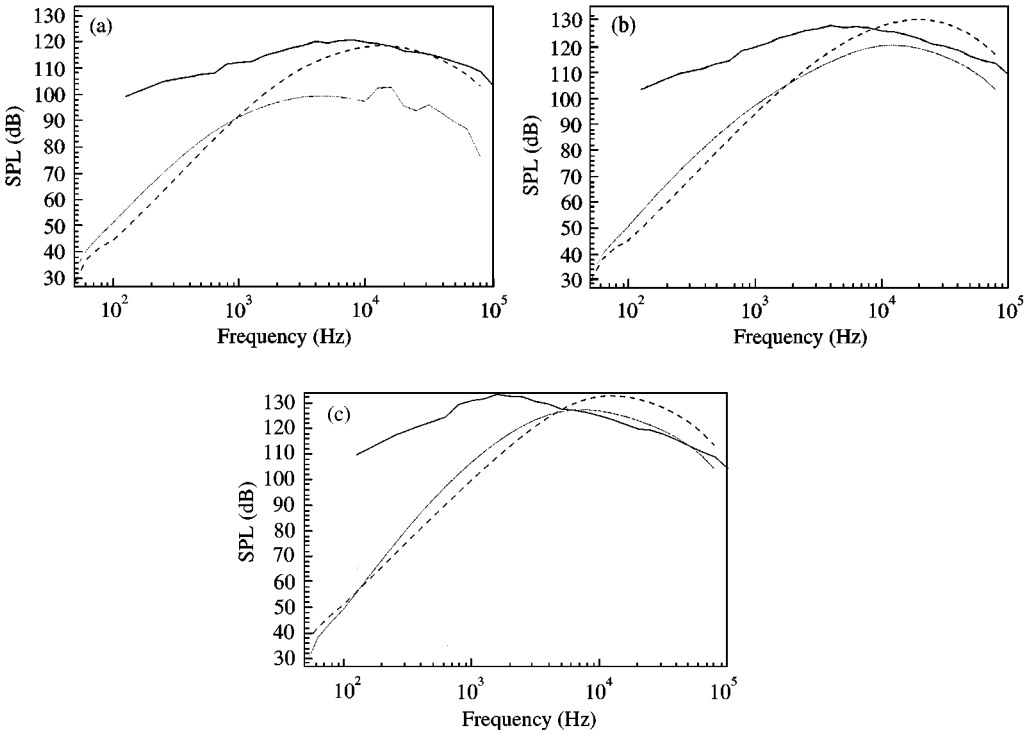

Figure 7. SPL at three microphone angles for 104°F case: ——, experiment; - - -, Khavaran MGB code; ···, present computation, using exponential spectrum and Kaneda time correlation (M + K). The source spectrum has been multiplied by a numerical factor that brings its peak value to that of the MGB source spectrum. (a) $\theta = 93{\cdot}3^\circ$, (b) $\theta = 122{\cdot}7^\circ$ and (c) $\theta = 138{\cdot}8^\circ$.

frequency bands varies differently with the angle θ, and so the results using the new spectrum exhibit different angular dependence than those using the original spectrum.) Both computations severely underpredict the low-frequency noise.

Results using the source spectrum of equation (25) from the M + K velocity correlation are shown in Figure 7. Most of the observations on the K + K results apply here as well, with the exception that the overall magnitudes of the M + K SPLs are somewhat more in line with the MGB and experimental results — this is most likely simply a result of the reduced amplitude discrepancy in the M + K source spectrum. In particular, the broadening of the SPL seen in the K + K results is even more pronounced here.

In order to separate out the effect of the shapes of the new source spectrum distributions from the effect of their overall amplitude, additional computations were carried out with each source spectrum multiplied by a factor which brings its peak value to the peak value of the MGB source spectrum. The results are shown in Figures 8 and 9. While there is improvement (the multiplicative factor makes the source-spectrum component large enough to cover the shock-noise component that generated the isolated peaks at $\theta = 93{\cdot}3^\circ$, for example), the predictions are still inadequate, particularly at higher values of θ. It is

Figure 9. SPL at three microphone angles for 104°F case: ——, experiment; ---, Khavaran MGB code; ···, present compution, using exponential spectrum and Kaneda time correlation (M + K). The source spectrum has been multiplied by a numerical factor that brings its peak value to that of the MGB source spectrum. (a) $\theta = 93{\cdot}3^\circ$, (b) $\theta = 122{\cdot}7^\circ$ and (c) $\theta = 138{\cdot}8^\circ$.

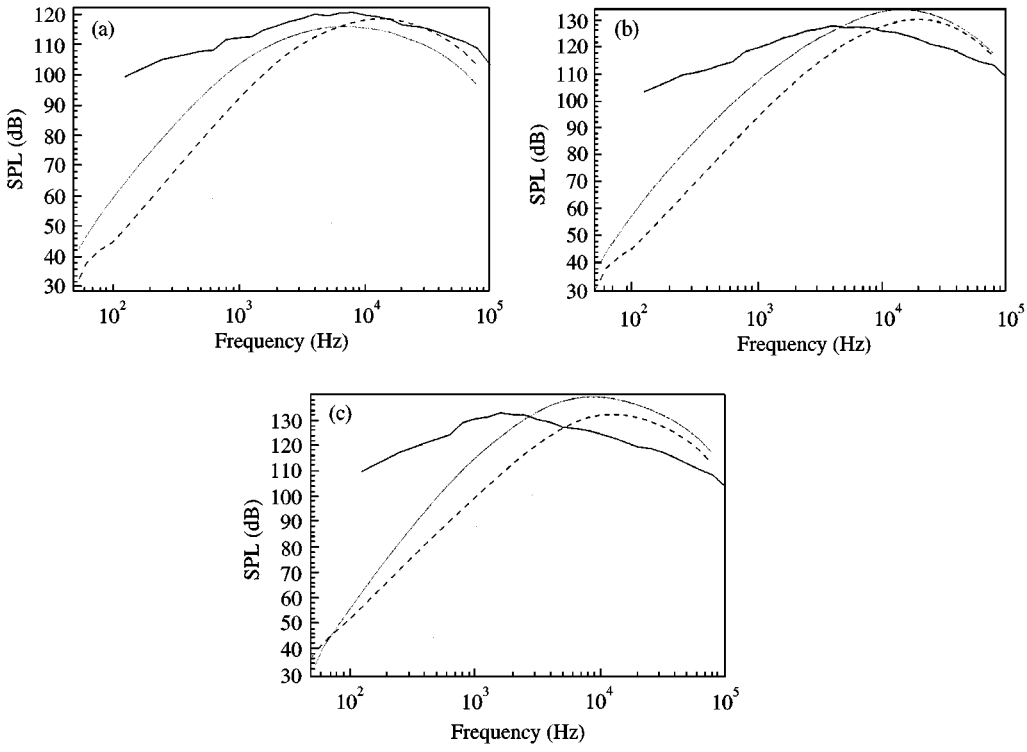

Figure 8. SPL at three microphone angles for 104°F case: ——, experiment; ---, Khavaran MGB code; ···, present compution, using Kolmogorov spectrum and Kaneda time correlation (K + K). The source spectrum has been multiplied by a numerical factor that brings its peak value to that of the MGB source spectrum. (a) $\theta = 93{\cdot}3^\circ$, (b) $\theta = 122{\cdot}7^\circ$ and (c) $\theta = 138{\cdot}8^\circ$.

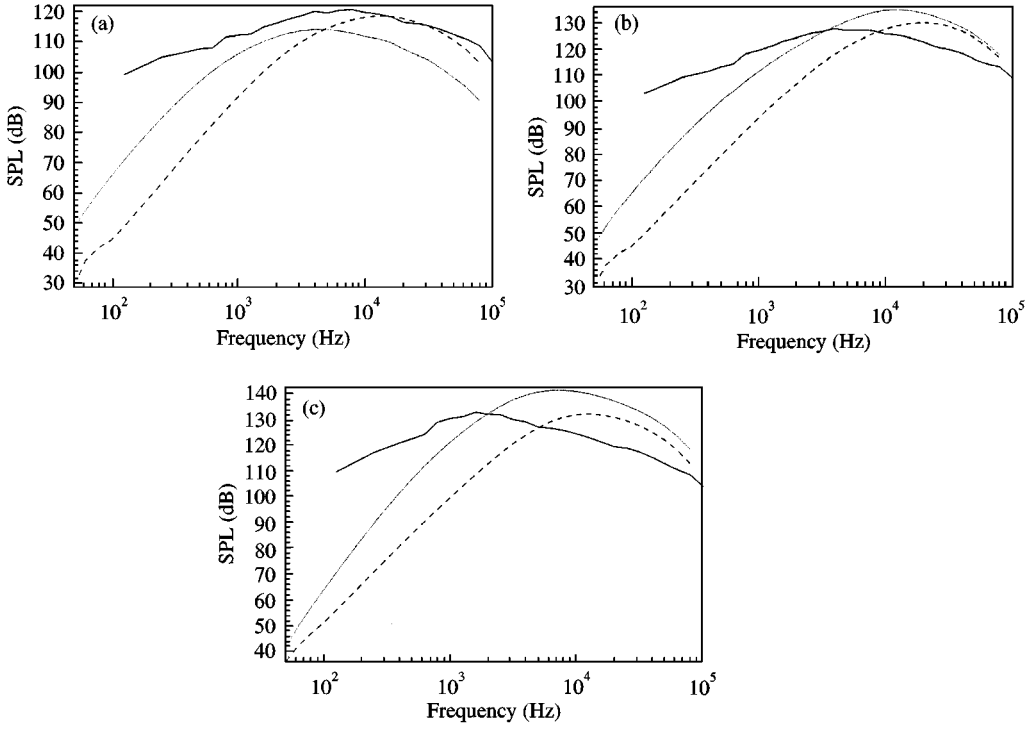

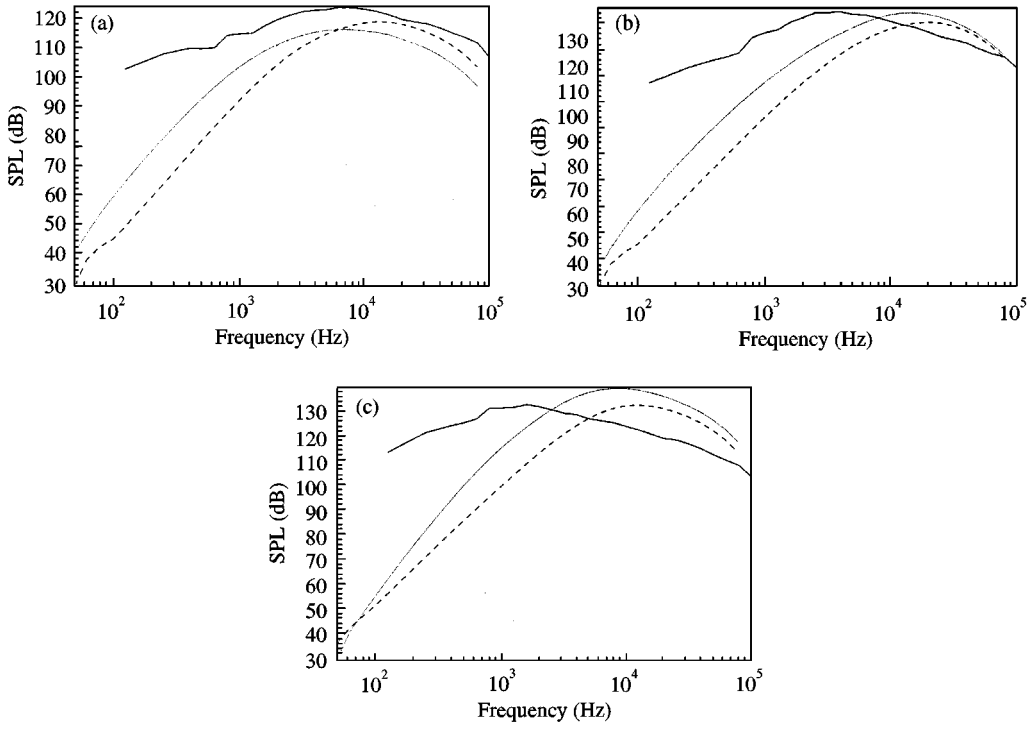

Figure 10. SPL at three microphone angles for 1550°F case: ——, experiment; ---, Khavaran MGB code; ···, present compution, using Kolmogorov spectrum and Kaneda time correlation (K + K). The source spectrum has been multiplied by a numerical factor that brings its peak value to that of the MGB source spectrum. (a) $\theta = 93{\cdot}3°$, (b) $\theta = 122{\cdot}7°$ and (c) $\theta = 138{\cdot}8°$.

interesting to note that the sensitivity of the K + K and M + K results in Figures 8 and 9 to variations in θ are significantly greater than that of the MGB results or the results in Figures 6 and 7.

The corresponding results for the two new spectra for the 1550°F jet case are shown in Figures 10 and 11. (These results are computed with the source spectra multiplied by the same factors as for Figures 8 and 9.) The qualitative trends are similar to those for the 104°F case.

While the two new source spectra examined here were derived from fairly crude representations of the turbulence velocity correlations and did not lead to a material improvement over the standard MGB code, the present results do show that the adoption of alternative velocity correlations can affect noise predictions. It is possible that further work in this direction will lead to improvements in MGB-code acoustic predictions, notwithstanding the poor performance of the spectra tried here. Consequently, more sophisticated velocity correlations are currently being investigated.

ACKNOWLEDGMENTS

The assistance of A. Khavaran in providing us with his code and in guiding us in its use is gratefully acknowledged. This research was supported by NASA through the NASA Langley Research Center.

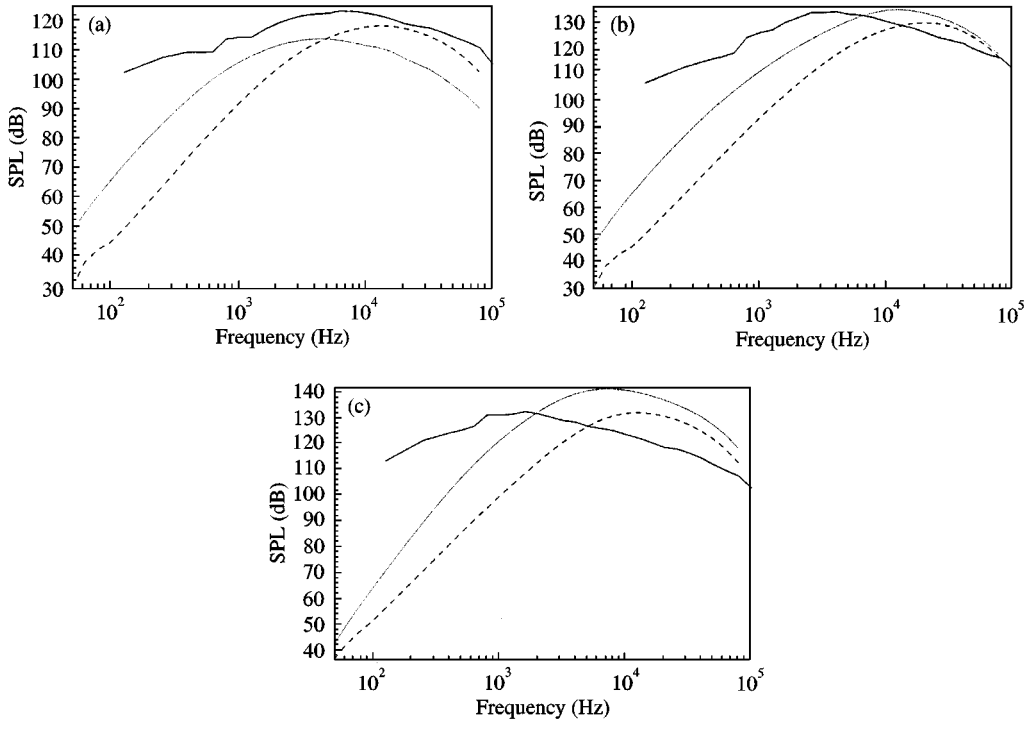

Figure 11. SPL at three microphone angles for 1550°F case: ——, experiment; ---, Khavaran MGB code; ···, present compution, using exponential spectrum and Kaneda time correlation (M + K). The source spectrum has been multiplied by a numerical factor that brings its peak value to that of the MGB source spectrum. (a) $\theta = 93{\cdot}3^\circ$, (b) $\theta = 122{\cdot}7^\circ$ and (c) $\theta = 138{\cdot}8^\circ$.

REFERENCES

1. J. M. Seiner 1997 *Theoretical and Computational Fluid Dynamics* **12**, 322–334. Jet noise reduction.
2. M. J. Lighthill 1952 *Proceedings of the Royal Society London* **A 211**, 564–587. On sound generated aerodynamically I. General theory.
3. A. Khavaran 1993 *AIAA Journal of Aircraft* **31**, 603–612. Computation of supersonic jet mixing noise for an axisymmetric convergent-divergent nozzle.
4. G. M. Lilley 1972 *Air Force Aero Propulsion Laboratory Technical Report* 72–53. The generation and radiation of supersonic jet noise. Vol. IV — theory of turbulence generated jet noise, noise radiation from upstream sources, and combustion noise. Part II: generation of sound in a mixing region.
5. J. E. Ffowcs-Williams 1963 *Philosophical Transactions of the Royal Society London* **B 255**, 469–503. The noise from turbulence convected at high speed.
6. R. Mani *et al.* 1977 *Task* 2, *FAA-RD*-76-79-*II*. High-velocity jet noise source location and reduction.
7. H. S. Ribner 1969 *Journal of Fluid Mechanics* **38**, 1–24. Quadrapole correlations governing the pattern of jet noise.
8. J. O. Hinze 1975 *Turbulence*. New York: McGraw-Hill, second edition.
9. J. M. Seiner, M. K. Ponton, B. J. Jansen and N. Lagen 1992 *DGLR/ AIAA* 14th *Aeroacoustics Conference*, *Aachen*, *Germany*, *Paper no.* 92-02-046. The effects of temperature on supersonic jet noise emission.
10. S. L. Woodruff, J. M. Seiner, M. Y. Hussaini and G. Erlebacher 1998 *AIAA Paper* 98-0083; expanded version accepted by *AIAA Journal*. Evaluation of turbulence-model performance as applied to jet-noise prediction.
11. Y. Kaneda 1981 *Journal of Fluid Mechanics* **107**, 131. Renormalized expansions in the theory of turbulence with the use of the Lagrangian position function.

12. Y. ZHOU and R. RUBINSTEIN 1996 *Physics of Fluids* **8**, 647. Sweeping and straining effects in sound generation by high Reynolds number isotropic turbulence.
13. R. RUBINSTEIN and Y. ZHOU 1999 *ICASE Report* 99-39, *European Journal of Mechanics B*, (submitted). Characterization of sound radiation by unresolved scales of motion in computational acoustics.
14. R. RUBINSTEIN and Y. ZHOU 2000 *Physics Letters A*. The frequency spectrum of sound represented by isotropic turbulence (to appear).
15. Y. ZHOU, E. HAYDER and R. RUBINSTEIN 2000 *Journal of Aircraft*. A model for radiated sound from high Reynolds number turbulence sources (submitted).
16. C. K. W. TAM and L. AURIAULT 1999 *AIAA Journal* **37**, 145–153. Jet mixing noise from fine-scale turbulence.
17. J. H. MORRISON 1992 *NASA CR* 4440. A compressible Navier–Stokes solver with two-equation and Reynolds-stress turbulence closure models.
18. D. C. WILCOX 1993 *Turbulence Modeling for CFD*. LaCanada, CA: DCW Industries, Inc.
19. R. H. KRAICHNAN 1959 *Journal of Fluid Mechanics* **5**, 497–543. The structure of turbulence at very high Reynolds numbers.
20. K. R. SREENIVASAN 1995 *Physics of Fluids* **7**, 2778–84. On the universality of the Kolmogorov constant.